Limitations of Reluctance Networks to Model the Frequency-Dependent Leakage and Fringing Fluxes in Active Magnetic Thrust Bearings

Robert SEIFERT

VEM Sachsenwerk GmbH, Pirnaer Landstraße 176, 01257 Dresden, Germany, robert.seifert@vem-group.com

Abstract

Previous works have demonstrated that analytical high–fidelity models of nonlaminated actuators and magnetic thrust bearings cannot just describe the magnetic skin effect inside the solid core, but also be applied directly within the control circuit. By an appropriate rational approximation a digital implementation on a microcontroller becomes possible. These approximated models generally do not consider frequency–dependent fringing and leakage fluxes, which may account for more than 7 % of the total flux. Reluctance networks are a popular choice to address this discrepancy. When calculated carefully, they can highly improve the accuracy of static models. However, their limitations in real–world scenarios are usually not discussed, even though the magnetic skin effect significantly changes the flux distribution in the nonlaminated core at already very low frequencies. In this article we review the practicability of reluctance networks and their possible simplifications in the context of real–time control systems. Depending on the control's objective we find they may be even discouraged, while simple correction factors allow for consistent results over the entire frequency range.

Keywords: Leakage Fluxes, Reluctance Networks, Eddy Currents, Active Magnetic Thrust Bearings, FO–Systems

1. Introduction

In recent years active magnetic bearings (AMBs) have seen an increase in their industrial applications due to a reduction in costs of the required power electronics and controllers but also in maintenance and operations, due to the establishment of remote service. This opens the market for new applications and prompts an increasing number of OEMs of traditional products, such as compressors, pumps and turbines to consider AMBs. As a consequence, there emerges a desire for high–stiffness AMBs with a disturbance suppression $\Delta K_{\mathrm{DS}} > 120\,\mathrm{dB}\frac{\mathrm{m}}{\mathrm{N}}$, which will match the stiffness of their mechanical counterparts ($\Delta K_{\mathrm{DS}} \approx 160\,\mathrm{dB}\frac{\mathrm{m}}{\mathrm{N}}$) to some degree. This is especially challenging for active magnetic thrust bearings (AMTB) as well as other solid–core actuators, as eddy current flow inside the core and the resultant magnetic skin effect is usually not avoidable (Seifert et al., 2021a).

The magnetic skin effect causes a significant lag between the force–generating magnetic flux and the measurable coil current, which results into a substantial damping of the actuator force in the often current controlled systems (Zhu et al., 2010). Alternatives, like a direct voltage control (Vischer, 1988) as well as hybrid forms (Ferreira et al., 2017; Keith, 1993) have not become established widely, considered only as a compromise. In previous works, we proposed a non–compromising control approach (Seifert et al., 2021a): instead of the measurable coil current, we control the actual force–generating flux as shown in Fig. 1. In the feedback branch we introduced a fractional–order flux estimator, which is able to determine the air gap flux from the measurable coil current in real–time. By use of the diffusion equation, the flux estimator mainly compensates the consequences of the magnetic skin effect caused by the eddy currents, but other nonlinearities may be considered as well. While the hysteresis is deemed neglectable, the core saturation can only be taken in account by a linearizing the core's permeability at a carefully determined operating point. Lastly, the inclusion of leakage and fringing fluxes is discussed in this paper. We review the practicability of reluctance networks as obvious choice often proposed in literature (e g. Le et al. (2016) and Sun et al. (2009) amongst others).

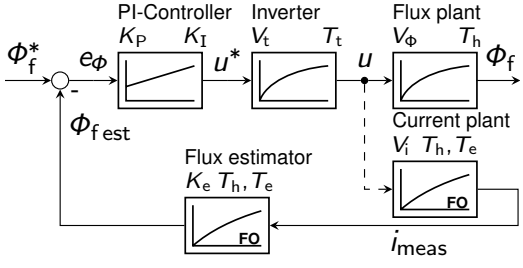

Figure 1: Closed–loop flux control with fractional–order flux estimator based on the measured coil current i_{meas}

Fringing and leakage fluxes are commonly subject of investigation in actuator modeling. However, in case of nonlaminated actuators like magnetic thrust bearings their accurate computation

is challenging and the authors find that – more often than not – approaches found in the literature are based on oversimplified assumptions. Usually, reluctance networks calculated for the magnetostatic case are also applied to the frequency domain, without discussing the impact of a changing flux distribution due to the magnetic skin effect. That is why we review the common practice of reluctance networks for the dynamic case of nonlaminated actuators. We use of a revised set of analytical expressions we proposed in Seifert et al., 2021b to model the reluctances of the fringing and leakage flux paths more accurately. In addition, possible simplifications are suggested to include leakage and fringing fluxes in real–time control models and distinguish them depending on the control's objective.

This paper is organized as follows. Section 2 gives a brief introduction into the existing eddy–current model, on which the flux model and estimator is based on. For a deeper understanding of the physics and the mathematical modeling based on fractional–order systems, we like to refer to our previous work Seifert et al., 2019. In the main part of the article we use a FE–analysis (FEA) to identify all flux paths and form a reluctance network for the static case in section 3. The inverted model can then be used in section 4 to calculate all frequency–dependent fringing/leakage fluxes for a given magnetomotive force. In the final section 5 we discuss the accuracy of the reluctance model and its actual practicability in comparison with simple constant correction factors.

2. Eddy current effects and their modeling

Eddy currents in nonlaminated actuators have already been discussed thoroughly in the literature in recent years. The foundations of any high–fidelity model in the frequency–domain were laid down by Stoll, 1974, further refined by Feeley, 1996 to establish the so–called "*eddy–inductance*", which we used for the flux estimator. Cylindrical actuators and magnetic bearings were first considered by Rabinovici et al., 1992 and Kucera et al., 1996, respectively, leading to the almost complete model by Zhu et al., 2010.

In our previous work (Seifert et al., 2019) we presented a full historical review of eddy current models, a study on their physical impact as well as final model refinements. Due to this extensive groundwork we will introduce only the most essential equations here.

In a first step, we divide the actuator geometry (Fig. 2) into core parts, which are only permeated by a one–dimensional magnetic flux $\underline{\Phi}_i(\mathrm{j}\omega)$. This we calculate by solving the diffusion equation $\mathrm{curl}\left(\mathrm{curl}\,\vec{\underline{B}}\right) = -\underline{\alpha}^2\vec{\underline{B}}$ in its complex form for every core element, where $\underline{\alpha} = \sqrt{\mathrm{j}\omega\kappa\mu}$ denotes the complex wave propagation constant with the constant permeability $\mu = \mu_0\mu_\mathrm{r}$ and electrical conductivity κ (for assumed isotropic and homogeneous materials). By help of the magnetomotive force (mmf) $\underline{\Theta}(\mathrm{j}\omega)$, we obtain the overall *effective reluctance* $\underline{\mathcal{R}}_\mathrm{eff}(\mathrm{j}\omega)$ as the sum of the part reluctances $\underline{\mathcal{R}}_i(\mathrm{j}\omega)$ of every core element $\underline{\mathcal{R}}_\mathrm{eff}(\mathrm{j}\omega)$, which translates into the *effective inductance* $\underline{L}_\mathrm{eff}(\mathrm{j}\omega)$ and the definition of the desired flux estimator:

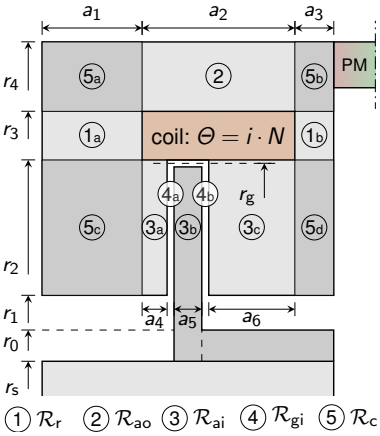

Figure 2: Magnetic circuit of AMTB divided into five classes of effective reluctances (cf. Seifert et al., 2019)

$$\underline{\mathcal{R}}_\mathrm{eff}(\mathrm{j}\omega) = \frac{N^2}{\underline{L}_\mathrm{eff}(\mathrm{j}\omega)} = \sum_i \frac{\underline{\Theta}(\mathrm{j}\omega)}{\underline{\Phi}_i(\mathrm{j}\omega)} = \sum_i \underline{\mathcal{R}}_i(\mathrm{j}\omega) \quad \Rightarrow \quad \underline{G}_\mathrm{FE}(\mathrm{j}\omega) = \frac{\Phi_\mathrm{fest}(\mathrm{j}\omega)}{\underline{i}_\mathrm{meas}(\mathrm{j}\omega)} = \frac{L_\mathrm{h}}{N}\frac{R_\mathrm{Cu} + s\underline{L}_\mathrm{eff}(\mathrm{j}\omega)}{R_\mathrm{Cu} + sL_\mathrm{h}}, \quad (1)$$

with the number of coil turns N. The main inductance $L_\mathrm{h} = L_\mathrm{eff}(\omega = 0)$ corresponds to the force–generating component of current and flux, which is independent from the eddy currents.

3. Static Fringing and Leakage Flux Model

The basis for every dynamic model of fringing Φ^υ and leakage fluxes Φ^σ is a magnetostatic model. For the sake of readability we speak of *non–core fluxes* $\Phi^{\upsilon|\sigma}$ covering both flux types as opposed to the core or *main path fluxes* exclusively permeating through the iron core and the geometrical air gap. Air gap fluxes Φ_gi, directly crossing the gap without bulging, are attributed to the core fluxes, as they share a comparable frequency behavior. Early adaptations of reluctance networks considering non–core fluxes in radial magnetic bearings go back to Meeker et al. (1996). Later they have been applied to thrust bearings by Sun et al., 2009 and Wang et al., 2014 as well as combined bearings by Le et al., 2016 and Zhong et al., 2017, like in our case, but with significantly differing leakage

paths and sometimes only for the magnetostatic case. Non–core fluxes in laminated radial bearings and conventional rotating machines are usually subject to only minor fluctuations and can be considered by a constant leakage k_σ and fringing factor k_υ, respectively. In nonlaminated AMTBs the magnetic skin effect alters the flux paths and the overall impact of the non–core fluxes depends on the frequency. For this reasons, we study the potential and practicability of a reluctance network and check whether it can be implemented within the flux estimator.

As a first step we assume a symmetrical thrust bearing (Fig. 3, bias flux omitted), to simplify the identification of the non–core flux paths in the field results of a magnetostatic FEA. Otherwise, negligible but misleading asymmetrical compensation fluxes occur. After identifying the reluctance network we calculate quantitative values for the non–core reluctances $\mathcal{R}^{\upsilon|\sigma}$. To achieve this, we use the fluxes determined for every network branch by the FEA for a given magnetomotive force (mmf) Θ. In section 4, the same network can then be used backwards to calculate the dynamic flux distribution for various frequencies and the real asymmetrical thrust bearing (cf. Fig. 2).

Generally, in thrust bearings we can differ between fringing and leakage fluxes as well as passive non–core fluxes. The latter have no influence on the force, as they do not bypass any air gaps. On the other hand, fringing fluxes bypass a single air gap in the direction of the force and therefore contribute to it. Leakage fluxes permeate perpendicular to the force or bypass both air gaps and are not part of the force generating main flux Φ_h. The following core Φ, fringing Φ^υ and leakage fluxes Φ^σ can be identified unambiguously from the FEA in Fig. 3:

a) Core and Air Gap Fluxes

- Φ_ao closes main flux path outside of coil in the outer stator and defines the total flux Φ_t quantitatively.
- $\Phi_\mathrm{giL|R}$ cross the air gaps in the main flux path. They are the major force–generating fluxes.
- Φ_di crosses the disk and rotor and equals the force–generating main flux, after subtraction of Φ^σ_dc.

b) Fringing Fluxes Φ^υ

- $\Phi^\upsilon_\mathrm{dioL|R}$ bypass single coil–sided air gap.
- $\Phi^\upsilon_\mathrm{aiiL|R}$ bypass single shaft–sided air gap.

c) Leakage Fluxes Φ^σ

- $\Phi^\sigma_\mathrm{ciiL|R}$ bypass between single air gap and shaft, perpendicular to thrust force. They vanish for high frequencies.
- Φ^σ_dc bypasses whole disk and therefore both air gaps.
- $\Phi^\sigma_\mathrm{riL|R}$ leak from inner side of the radial core elements $\mathcal{R}_\mathrm{rL|R}$. They form negligible flux swirls, which alter their shape even for small changes of frequency, load or symmetry. To simplify the network calculation, they are neglected.

d) Passive non–core Fluxes

- $\Phi^\sigma_\mathrm{rcL|R}$ cross the coil through its center. Depending on the symmetry, they form swirls only for low frequencies. For high frequencies they change direction and exclusively bypass core elements with no direct impact on the force.

Every one of these non–core fluxes $\Phi^{\upsilon|\sigma}$ is assigned to a non–core reluctance $\mathcal{R}^{\upsilon|\sigma}$. In combination with the core reluctances $\mathcal{R}$ in Fig. 2 (calculated in Seifert et al., 2019) we obtain the complete reluctance network in Fig. 4.

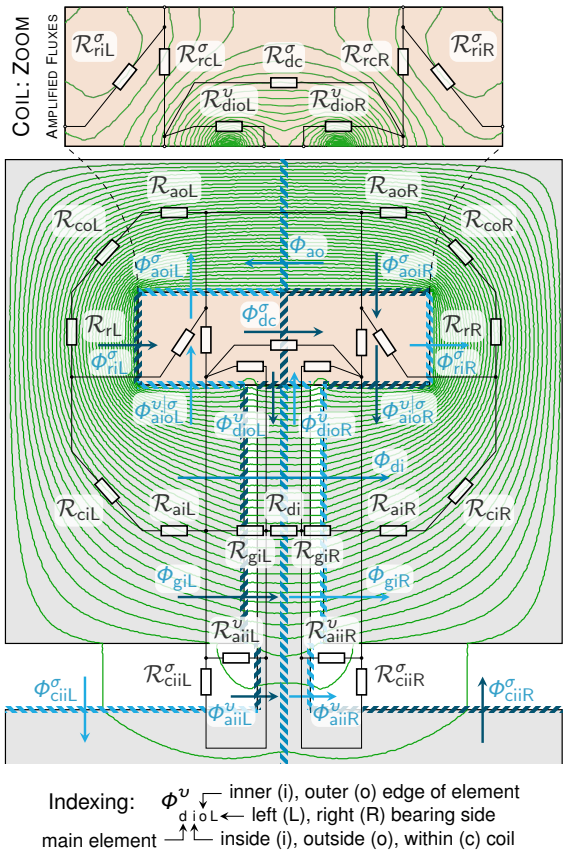

Figure 3: Magnetostatic flux distribution of symmetrical AMTB with omitted bias flux: Identification of fringing Φ^υ and leakage fluxes Φ^σ and reluctances from FEA

Physically, the mmf Θ is a distributed quantity and should be considered by a multitude of sources in the network. However, since the exact distribution is not known, it would increase the number of unknowns and the network could not be solved. Rather we place the mmf where the total magnetic flux Φ_t is at its maximum: in the outer stator yoke. To be able to model the swirls $\Phi^\sigma_\mathrm{rcL|R} = \Phi^\sigma_\mathrm{aoiL|R}$ (with $\Phi^\sigma_\mathrm{riL|R}$ neglected), we distribute Θ to the outer corners and the center of the stator (Fig. 4). However, to consider the changing directions of the fluxes $\Phi^\sigma_\mathrm{aoiL|R}$ and to keep the network solvable, the manually chosen weighting has to be adapted for the static and dynamic as well as symmetric and asymmetric case. We remind that in magnetic circuits a mesh is defined as $\sum \Theta_i = \sum \mathcal{R}_i \Phi_i$, so the sum of mmf sources equals the sum of magnetic voltage drops $\sum \mathcal{R}_i \Phi_i$.

Hence, the reluctance network is described by the system of linear equations $\mathcal{R}\cdot\boldsymbol{\Psi}=\boldsymbol{\Theta}$ with the reluctance matrix $\mathcal{R}$ as well as the vectors $\boldsymbol{\Psi}$ and $\boldsymbol{\Theta}$ describing the flux linkages of every mesh and the mmf sources, respectively. Using Kirchhoff's circuit laws, the flux linkages

$$\boldsymbol{\Psi}=\begin{bmatrix}\Psi_{\mathrm{rL}}\ \Psi_{\mathrm{rR}}\ \Psi_{\mathrm{ciI}}\ \Psi_{\mathrm{ciR}}\ \Psi_{\mathrm{giL}}\ \Psi_{\mathrm{giR}}\ \Psi_{\mathrm{goL}}\ \Psi_{\mathrm{goR}}\ \Psi_{\mathrm{c}}\ \Psi_{\mathrm{g}}\end{bmatrix}^{\mathrm{T}} \quad (2)$$

are calculated step–wise and the fluxes determined from the magnetostatic FE–analysis (as indicated in Fig. 3):

$$\begin{aligned}
\Psi_{\mathrm{ciL}}&=\Phi^{\sigma}_{\mathrm{ciiL}} & \Psi_{\mathrm{giL}}&=\Phi^{\upsilon}_{\mathrm{aiiL}}+\Phi^{\sigma}_{\mathrm{ciiL}}\\
\Psi_{\mathrm{ciR}}&=\Phi^{\sigma}_{\mathrm{ciiR}} & \Psi_{\mathrm{giR}}&=\Phi^{\upsilon}_{\mathrm{aiiR}}+\Phi^{\sigma}_{\mathrm{ciiR}}\\
\Psi_{\mathrm{c}}&=\Phi_{\mathrm{ao}} & \Psi_{\mathrm{goL}}&=\Phi_{\mathrm{ao}}-\Phi^{\sigma}_{\mathrm{dc}}-\Phi^{\upsilon}_{\mathrm{dioL}} \quad (3)\\
\Psi_{\mathrm{rL}}&=\Phi_{\mathrm{ao}}+\Phi^{\sigma}_{\mathrm{aoiL}} & \Psi_{\mathrm{goR}}&=\Phi_{\mathrm{ao}}-\Phi^{\sigma}_{\mathrm{dc}}-\Phi^{\upsilon}_{\mathrm{dioR}}\\
\Psi_{\mathrm{rR}}&=\Phi_{\mathrm{ao}}+\Phi^{\sigma}_{\mathrm{aoiR}} & \Psi_{\mathrm{g}}&=\Phi_{\mathrm{ao}}-\Phi^{\sigma}_{\mathrm{dc}}\quad .
\end{aligned}$$

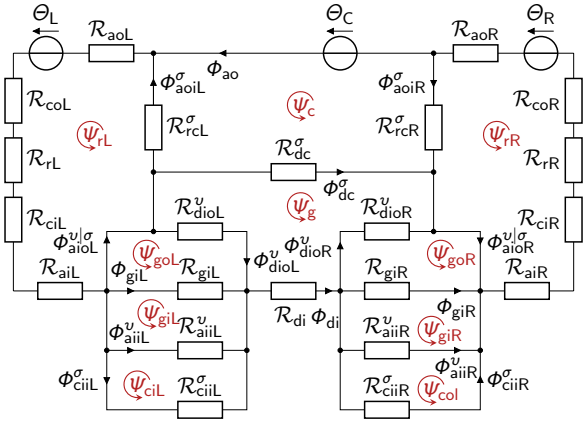

Figure 4: Complete reluctance network including fringing $\mathcal{R}^{\upsilon}_i$ and leakage reluctances $\mathcal{R}^{\sigma}_i$

With more equations the system would be overdetermined, so the focus lies on the total flux $\Phi_{\mathrm{ao}}=\Phi_{\mathrm{t}}$ which can be quantified exactly and defines the reference flux. For the static and symmetric case the mmf sources are distributed equally to the stator corners, to maintain the swirl character of $\Phi^{\sigma}_{\mathrm{aoiL|R}}$:

$$\Theta_{\mathrm{L}}=\Theta_{\mathrm{R}}=\Theta/2 \quad\text{and}\quad \Theta_{\mathrm{C}}=0 \quad\text{leading to the vector}\quad \boldsymbol{\Theta}=\begin{bmatrix}\Theta_{\mathrm{L}}\,\Theta_{\mathrm{R}}\,0\ \ 0\ \ 0\ \ 0\ \ 0\ \ 0\ \ \Theta_{\mathrm{C}}\ \ 0\end{bmatrix}^{\mathrm{T}}. \quad (4)$$

The reluctance matrix $\mathcal{R}$ describing the network is composed of the sought–after non–core reluctances $\mathcal{R}^{\upsilon|\sigma}_i$ as well as the known analytical solutions for the static part reluctances $\mathcal{R}_{0\,i}$ from Fig. 2. It is depicted in detail in Seifert et al., 2021b. To solve the equation system for all $\mathcal{R}^{\upsilon|\sigma}_i$ e. g. the Gaussian elimination algorithm or a computer algebra system (CAS) can be used. At this point we omit the last mesh equation for Ψ_{g}, as there are only nine unknown reluctances, but it is later needed for the backward calculation of the leakage fluxes from the network. The quantitative values of the determined non–core reluctances $\mathcal{R}^{\upsilon|\sigma}_i$ are summarized in Table 1 and compared with the parallel core reluctances $\mathcal{R}_{||}$ they bypass. It becomes apparent, that in the operational bandwidth of the thrust bearing (up to 1 kHz) the central leakage reluctances $\mathcal{R}^{\sigma}_{\mathrm{rcL|R}}$ have the least impact and can be neglected. On the other hand, a comparison of Table 1 with Fig. 5 shows that the high impact of the reluctances $\mathcal{R}^{\upsilon}_{\mathrm{aiiL|R}}$ and $\mathcal{R}^{\sigma}_{\mathrm{ciiL|R}}$ on the side of the shaft, with 7.8 % and 14 %, respectively, is misleading. The actual fluxes $\Phi^{\upsilon}_{\mathrm{aiiL|R}}$ and $\Phi^{\sigma}_{\mathrm{ciiL|R}}$ fall below 1 % for more than 1 kHz, due to the magnetic skin effect. This discrepancy can not be compensated by the reluctance network, as we will show later (cf. Fig. 8).

4. Dynamic Fringing and Leakage Flux Model

Already for frequencies below 1 Hz the magnetic skin effect causes the core fluxes to permeate closer to the coil. As a consequence, the leakage flux $\Phi^{\sigma}_{\mathrm{rcL|R}}$ change their direction, so the mmf–source has to be arranged centrally in the outer branch of the reluctance network in Fig. 4, such that $\Theta_{\mathrm{L}}=\Theta_{\mathrm{R}}=0$ and $\Theta_{\mathrm{C}}=\Theta$. In the fully computed reluctance network, we can now substitute the static part reluctances $\mathcal{R}_{0\,i}$ by the frequency–dependent, and therefore complex, effective part reluctances $\underline{\mathcal{R}}_i$ (Seifert et al., 2019). For a given mmf Θ it is then possible to calculate the mesh flux linkages $\underline{\Psi}$ and hence every core flux $\underline{\Phi}_i$ and non–core flux $\underline{\Phi}^{\upsilon|\sigma}$ for any frequency.

Table 1: Fringing $\mathcal{R}^{\upsilon}_i$ and leakage reluctances $\mathcal{R}^{\sigma}_i$ determined by FEA compared to bypassed core reluctances $\mathcal{R}_{||}$ (symmetric case)

$\mathcal{R}^{\upsilon\|\sigma}_i$	in A/Vs	$\mathcal{R}_{\|\|}$	in A/Vs	$\mathcal{R}_{\|\|}/\mathcal{R}^{\upsilon\|\sigma}_i$	
SYMMETRIC CASE:				0 Hz	1 kHz
$\mathcal{R}^{\sigma}_{\mathrm{rcL|R}}$	$2.36\cdot10^{7}$	$\mathcal{R}_{\mathrm{soL|R}}$	$1.08\cdot10^{4}$	0.05 %	2.06 %
$\mathcal{R}^{\upsilon}_{\mathrm{dioL|R}}$	$5.94\cdot10^{6}$	$\mathcal{R}_{\mathrm{giL|R}}$	$1.01\cdot10^{5}$	2.37 %	6.22 %
$\mathcal{R}^{\upsilon}_{\mathrm{aiiL|R}}$	$3.39\cdot10^{6}$	$\mathcal{R}_{\mathrm{giL|R}}$	$1.01\cdot10^{5}$	2.99 %	7.84 %
$\mathcal{R}^{\sigma}_{\mathrm{ciiL|R}}$	$1.89\cdot10^{6}$	$\mathcal{R}_{\mathrm{giL|R}}$	$1.01\cdot10^{5}$	5.36 %	14.06 %
$\mathcal{R}^{\sigma}_{\mathrm{dc}}$	$1.51\cdot10^{7}$	$\mathcal{R}_{\mathrm{di+giL+giR}}$	$2.03\cdot10^{5}$	1.34 %	4.18 %

*$\mathcal{R}_{\mathrm{soL|R}}=\mathcal{R}_{\mathrm{aoL|R}}+\mathcal{R}_{\mathrm{coL|R}}+\mathcal{R}_{\mathrm{rL|R}}+\mathcal{R}_{\mathrm{ciL|R}}+\mathcal{R}_{\mathrm{aiL|R}}$

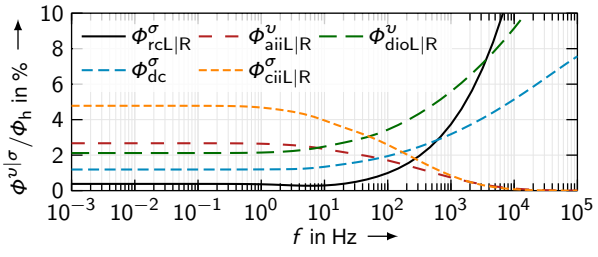

Figure 5: Share of fringing Φ^{υ} and leakage fluxes Φ^{σ} on the total flux $\Phi_{\mathrm{t}}=\Phi_{\mathrm{ao}}$ for the symmetric thrust bearing

This way, the sole analytical overall effective reluctance $\underline{\mathcal{R}}_{\mathrm{eff}}$ can be corrected to the leakage- and fringing–accounting effective reluctance $\underline{\mathcal{R}}'_{\mathrm{eff\,t}} = \Theta/\underline{\Phi}_{\mathrm{ao}} = \Theta/\underline{\Phi}_{\mathrm{t}}$, which we compare with a dynamic FEA. Fig. 6 shows, that the amplitude error of $\underline{\mathcal{R}}_{\mathrm{eff}}$ (ca. 1 dB) towards the FEA results can be eliminated almost entirely by the reluctance network. The leakage and fringing fluxes are also responsible for a considerable decay of the phase from its theoretical limit of 45 ° for high frequencies, which is describable by the network as well. Only the modeling error of the original analytical solution around the eddy current edge frequency f_{e} (cf. Seifert et al., 2019) persists.

4.1 Simplified dynamic reluctance network

The complexity of the complete network (Fig. 4) leads to a significant increase in the system order m_{S} of the rational form of $\underline{\mathcal{R}}_{\mathrm{eff}}$ (Seifert et al., 2019) and is therefore not applicable for the estimator G_{FE}. Hence, we propose the following simplifications, based on Table 1, Fig. 5 and the qualitative evaluation of the FEA field distribution.

1. The outer axial core reluctances $\underline{\mathcal{R}}_{\mathrm{aoL|R}}$ are summed up to $\underline{\mathcal{R}}_{\mathrm{ao}}$ by addition of their characteristic lengths.

2. The fringing fluxes $\underline{\Phi}^{\upsilon}_{\mathrm{dioL|R}}$, $\underline{\Phi}^{\upsilon}_{\mathrm{aiiL|R}}$ (and corresponding reluctances) are combined and assigned to the air gap fringing reluctances $\mathcal{R}^{\upsilon}_{\mathrm{giL|R}}$:

$$\mathcal{R}^{\upsilon}_{\mathrm{giL|R}} = \frac{\mathcal{R}^{\upsilon}_{\mathrm{dioL|R}}\,\mathcal{R}^{\upsilon}_{\mathrm{aiiL|R}}}{\mathcal{R}^{\upsilon}_{\mathrm{dioL|R}} + \mathcal{R}^{\upsilon}_{\mathrm{aiiL|R}}}\,. \tag{5}$$

3. The central leakage reluctance $\mathcal{R}^{\sigma}_{\mathrm{dc}}$, bypassing both air gaps, is divided into two equal parts, assigned to a single air gap each. Together with the leakage reluctance $\mathcal{R}^{\sigma}_{\mathrm{ciiL|R}}$ on the shaft side, they form the air gap leakage reluctances $\mathcal{R}^{\sigma}_{\mathrm{giL|R}}$:

$$\mathcal{R}^{\sigma}_{\mathrm{giL|R}} = \frac{\frac{1}{2}\mathcal{R}^{\sigma}_{\mathrm{dc}}\,\mathcal{R}^{\sigma}_{\mathrm{ciiL|R}}}{\frac{1}{2}\mathcal{R}^{\sigma}_{\mathrm{dc}} + \mathcal{R}^{\sigma}_{\mathrm{ciiL|R}}}\,. \tag{6}$$

4. To determine the corrected total effective reluctance $\underline{\mathcal{R}}'_{\mathrm{eff\,t}}$, relating to the total flux $\underline{\Phi}_{\mathrm{ao}} = \underline{\Phi}_{\mathrm{t}}$ and not considering the force, we merge $\mathcal{R}^{\upsilon}_{\mathrm{giL|R}}$ and $\mathcal{R}^{\sigma}_{\mathrm{giL|R}}$ to the combined air gap fringing and leakage reluctance $\mathcal{R}^{\upsilon\sigma}_{\mathrm{giL|R}}$:

$$\mathcal{R}^{\upsilon\sigma}_{\mathrm{giL|R}} = \frac{\mathcal{R}^{\upsilon}_{\mathrm{giL|R}}\,\mathcal{R}^{\sigma}_{\mathrm{giL|R}}}{\mathcal{R}^{\upsilon}_{\mathrm{giL|R}} + \mathcal{R}^{\sigma}_{\mathrm{giL|R}}}\,. \tag{7}$$

5. The respective “geometrical” air gap reluctances in the main flux path are equal for both bearing sides, independently from the symmetry, so that $\underline{\mathcal{R}}_{\mathrm{giL|R}} = \underline{\mathcal{R}}_{\mathrm{gi}}$. Furthermore we calculate the arithmetic mean of $\mathcal{R}^{\upsilon\sigma}_{\mathrm{giL|R}}$ to obtain the single corrected air gap reluctance:

$$\underline{\mathcal{R}}'_{\mathrm{gi}} = 2\left(\overline{\mathcal{R}}^{\upsilon\sigma}_{\mathrm{gi}} \,||\, \underline{\mathcal{R}}_{\mathrm{gi}}\right) \quad \text{with} \quad \overline{\mathcal{R}}^{\upsilon\sigma}_{\mathrm{gi}} = \frac{1}{2}\left(\mathcal{R}^{\upsilon\sigma}_{\mathrm{giL}} + \mathcal{R}^{\upsilon\sigma}_{\mathrm{giR}}\right) \tag{8}$$

The introduced error of $\underline{\mathcal{R}}'_{\mathrm{gi}}$ compared to $\underline{\mathcal{R}}_{\mathrm{giL|R}} \,||\, \mathcal{R}^{\upsilon\sigma}_{\mathrm{giL|R}}$ is only 0.03 %, which is why we also adopt this step for

$$\overline{\mathcal{R}}^{\upsilon}_{\mathrm{gi}} = \frac{1}{2}\left(\mathcal{R}^{\upsilon}_{\mathrm{giL}} + \mathcal{R}^{\upsilon}_{\mathrm{giR}}\right), \quad \overline{\mathcal{R}}^{\sigma}_{\mathrm{gi}} = \frac{1}{2}\left(\mathcal{R}^{\sigma}_{\mathrm{giL}} + \mathcal{R}^{\sigma}_{\mathrm{giR}}\right). \tag{9}$$

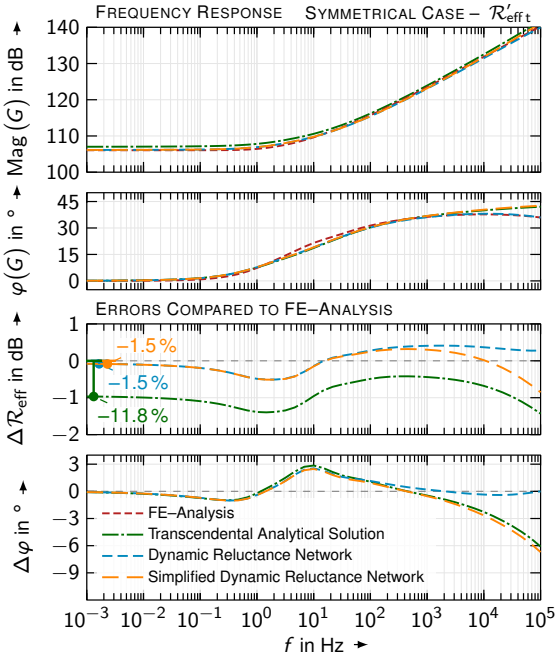

Figure 6: Frequency responses for the corrected total eff. reluctance $\mathcal{R}'_{\mathrm{eff\,t}}$ relating to the total flux Φ_{t} and its absol. magnitude- and phase errors in respect to reference FEA

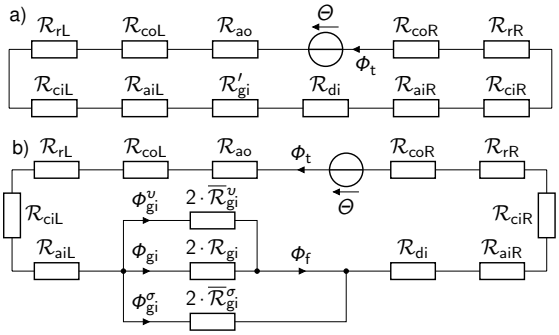

Figure 7: Simplified dynamic reluctance network with a) corrected air gap reluctance or b) with total flux path split into the force–generating fringing Φ^{υ} and leakage part Φ^{σ}

6. As a last step we neglect the transversal reluctances $\mathcal{R}^{\sigma}_{\mathrm{rcL|R}}$, since their impact for low frequencies is negligible (cf. Fig. 5). Although in the dynamic case for high frequencies above 1 kHz the respective fluxes $\underline{\Phi}^{\sigma}_{\mathrm{rcL|R}}$ are dominant, the impact of $\mathcal{R}^{\sigma}_{\mathrm{rcL|R}}$ on the magnitude response of $\underline{\mathcal{R}}'_{\mathrm{eff\,t}}$ is limited due its passive characteristic. However, the previously observed phase decay for frequencies above 1 kHz cannot be modeled without $\mathcal{R}^{\sigma}_{\mathrm{rcL|R}}$, which is deemed uncritical, as it lies outside of the bearings operating bandwidth. If higher bandwidths require the consideration of $\mathcal{R}^{\sigma}_{\mathrm{rcL|R}}$, one should be aware that the system order m_{S} almost doubles.

As result we obtain the simplified dynamic reluctance network in Fig. 7, which forms the leakage- and fringing–accounting total effective reluctance $\underline{\mathcal{R}}'_{\mathrm{eff\,t}} = \Theta/\underline{\Phi}_{\mathrm{t}}$ by summing up of its part reluctances. Up to ca. 100 Hz both, the full and the simplified network, lead to identical results. In the further relevant bandwidth up to 1 kHz the magnitude and phase error remains low with < 0.4 dB and $< 1\,°$, respectively (cf. Fig. 6).

However, in this form the network cannot just yet be applied to the flux estimator, as the magnetic bearing control relies on the force–generating main flux $\underline{\Phi}_{\mathrm{h}} = \underline{\Phi}_{\mathrm{f}} = \underline{\Phi}_{\mathrm{gi}} + \underline{\Phi}^{\upsilon}$ and not the total flux $\underline{\Phi}_{\mathrm{t}}$ as illustrated in Fig. 7. Consequentially, the force–related total effective reluctance $\underline{\mathcal{R}}'_{\mathrm{eff\,f}} = \Theta/\underline{\Phi}_{\mathrm{f}}$ only refers to the force–generating flux $\underline{\Phi}_{\mathrm{f}}$. The results for the accordingly adapted $\underline{\mathcal{R}}'_{\mathrm{eff\,f}}$ will be shown in section 4.3

4.2 Transition to Asymmetric Bearing

In the asymmetric real thrust bearing the position of the coil was shifted to the right as depicted in Fig. 2. We took this measure to equalize the static reluctances of the bias flux paths and therefore enable equal forces in both air gaps. In terms of fringing and leakage fluxes, we observe that they are facilitated for high frequencies $f > 1$ kHz especially on the left side of the bearing (Seifert et al., 2021b). Furthermore, the right–sided central leakage flux $\underline{\Phi}^{\sigma}_{\mathrm{aoiR}}$ remains a swirl, as in Fig. 4, over the entire frequency range, while its left–sided counterpart $\underline{\Phi}^{\sigma}_{\mathrm{aoiL}}$ is always passive (it changes its direction compared to Fig. 4). To account for this asymmetry, the magnetic voltage source has to be placed in the outer right corner of the network, such that $\Theta_{\mathrm{L}} = \Theta_{\mathrm{C}} = 0$ and $\Theta_{\mathrm{R}} = \Theta$. By this slight adjustment, the full and the simplified reluctance network enables comparable results for the corrected total effective reluctance $\underline{\mathcal{R}}'_{\mathrm{eff\,t}}$ like in the symmetric case, at least in the bandwidth below 1 kHz. Quantitative error data is disclosed in Seifert et al., 2021b.

4.3 Implementation and Conclusion

Previously we indicated, that for the flux estimator not only the corrected total effective reluctance $\underline{\mathcal{R}}'_{\mathrm{eff\,t}} = \Theta/\underline{\Phi}_{\mathrm{t}}$ is decisive, but also the force–related effective reluctance $\underline{\mathcal{R}}'_{\mathrm{eff\,f}} = \Theta/\underline{\Phi}_{\mathrm{f}}$. The latter relates solely to the actual force–generating part $\underline{\Phi}_{\mathrm{f}}$ of the total flux $\underline{\Phi}_{\mathrm{t}}$, which we calculate with the flux divider following Fig. 7. By dividing both fluxes, $\underline{\Phi}_{\mathrm{f}}$ and $\underline{\Phi}_{\mathrm{t}}$, through the mmf $\Theta = i \cdot N$ and calculating the reciprocal, we obtain the desired form:

$$\underline{\Phi}_{\mathrm{f}} = \frac{\mathcal{R}^{\sigma}_{\mathrm{gi}}}{\mathcal{R}^{\sigma}_{\mathrm{gi}} + \underline{\mathcal{R}}_{\mathrm{gf}}}\,\underline{\Phi}_{\mathrm{t}} \quad \text{with} \quad \underline{\mathcal{R}}_{\mathrm{gf}} = 2\,\frac{\overline{\mathcal{R}}^{\upsilon}_{\mathrm{gi}}\,\underline{\mathcal{R}}_{\mathrm{gi}}}{\overline{\mathcal{R}}^{\upsilon}_{\mathrm{gi}} + \underline{\mathcal{R}}_{\mathrm{gi}}} \quad \text{and} \quad \mathcal{R}^{\sigma}_{\mathrm{gi}} = 2\,\overline{\mathcal{R}}^{\sigma}_{\mathrm{gi}} \quad \overset{:\,\Theta}{\Longrightarrow} \quad \underline{\mathcal{R}}'_{\mathrm{eff\,f}} = \left(1 + \frac{\underline{\mathcal{R}}_{\mathrm{gf}}}{\mathcal{R}^{\sigma}_{\mathrm{gi}}}\right)\underline{\mathcal{R}}'_{\mathrm{eff\,t}}\,. \tag{10}$$

The implementation of the combined air gap leakage reluctances $\mathcal{R}^{\upsilon\sigma}_{\mathrm{giL|R}}$, leading to $\underline{\mathcal{R}}'_{\mathrm{eff\,t}}$, is carried out together with the calculation of the air gap reluctance $\underline{\mathcal{R}}_{\mathrm{gi}}$ or the air gap element (fractional order $\gamma = 1/4$) of the equivalent implicit system $\underline{\mathcal{R}}_{\mathrm{EIS}}$ (cf. Seifert et al., 2019, eq. (58)) according to (8). In the next step, we derive the force–related reluctance $\underline{\mathcal{R}}'_{\mathrm{eff\,f}}$ from (10). All subsequent calculations affect neither the approximations nor the discretization. Only the system orders $m_{\mathrm{S}}, n_{\mathrm{S}}$ of the approximated overall system (sum of all part reluctances in Fig. 7 or equivalent implicit system Seifert et al., 2019) increase – in case of $\underline{\mathcal{R}}'_{\mathrm{eff\,t}}$ only by 1, regarding $\mathcal{R}'_{\mathrm{eff\,f}}$, the flux divider implicates a further increase of the total order by the order $m_{\mathcal{R}_{\mathrm{g}}}$ of the reluctance $\underline{\mathcal{R}}_{\mathrm{gi}}$:

$$m_{\mathrm{St}} = m_{\mathrm{S}} + 1, \quad n_{\mathrm{St}} = m_{\mathrm{St}} - 1 \qquad \text{vs.} \qquad m_{\mathrm{Sf}} = m_{\mathrm{S}} + m_{\mathcal{R}_{\mathrm{g}}} + 1 = m_{\mathrm{St}} + m_{\mathcal{R}_{\mathrm{g}}}, \quad n_{\mathrm{Sf}} = m_{\mathrm{Sf}} - 1\,. \tag{11}$$

However, in Seifert et al., 2019 we proposed to undertake an additional Padé–approximation (PASR), which overrides the increase in order of $m_{\mathcal{R}_{\mathrm{g}}} = 8 \ldots 29$ (for $f < 21$ kHz). Therefore, the order of the PASR–solution $m_{\mathcal{P}}$ remains equal to the fringing/leakage–free model. This is a considerable advantage compared to the other proposed approximation method MAEIS, where considering the leakage within $\underline{\mathcal{R}}'_{\mathrm{eff\,f}}$ increases the total system order by $m_{\mathcal{R}_{\mathrm{g}}} = (m_{\mathrm{S}} + 1)/2 = 5 \ldots 25$, limiting the applicability of the approach.

5. Alternative: Constant Correction Factor

The simplest way to take fringing and leakage fluxes into account, is the introduction of constant correction factors $k_{\upsilon\sigma\mathrm{t}}$ and $k_{\upsilon\sigma\mathrm{f}}$ (relating to the current i). Without an increase to the system order, we can correct the total effective reluctance $\underline{\mathcal{R}}_{\mathrm{eff}}$ or inductance $\underline{L}_{\mathrm{eff}}$ with the correction factor $k_{\upsilon\sigma\mathrm{t}}$, by forming the ratio of the static corrected overall reluctance $\mathcal{R}'_{0\mathrm{t}}$ with the static fringing/leakage–free reluctance $\mathcal{R}_0 = \mathcal{R}_{\mathrm{eff}}(f = 0)$:

$$\underline{L}_{\mathrm{eff\,t}} = k_{\upsilon\sigma\mathrm{t}} N \frac{\underline{\Phi}_{\mathrm{t}}}{i} = \frac{k_{\upsilon\sigma\mathrm{t}} N^2}{\underline{\mathcal{R}}_{\mathrm{eff}}} = \frac{N^2}{\underline{\mathcal{R}}'_{\mathrm{eff\,t}}} \;\Rightarrow\; \underline{\mathcal{R}}'_{\mathrm{eff\,t}} = \frac{\underline{\mathcal{R}}_{\mathrm{eff}}}{k_{\upsilon\sigma\mathrm{t}}} \qquad \Rightarrow \qquad k_{\upsilon\sigma\mathrm{t}} = \frac{\mathcal{R}_0}{\mathcal{R}'_{0\mathrm{t}}} = \mathcal{R}_0 \cdot \frac{\Phi_{0\mathrm{t}}}{\Theta}\,, \tag{12}$$

The determination of $\mathcal{R}_{0\mathrm{t}}$ in (10) or Φ_t for that matter, can be conducted by analytical calculation or a FEA. By using the flux divider from (10) we determine analogously the force–related effective inductance and the corresponding correction factor $k_{\upsilon\sigma\mathrm{f}}$:

$$\underline{L}_{\mathrm{eff\,f}} = k_{\upsilon\sigma\mathrm{f}} N \frac{\underline{\Phi}_\mathrm{f}}{i} = \frac{k_{\upsilon\sigma\mathrm{f}} N^2}{\underline{\mathcal{R}}_\mathrm{eff}} = \frac{N^2}{\underline{\mathcal{R}}'_{\mathrm{eff\,f}}} \Rightarrow \underline{\mathcal{R}}'_{\mathrm{eff\,f}} = \frac{\underline{\mathcal{R}}_\mathrm{eff}}{k_{\upsilon\sigma\mathrm{f}}} \quad \Rightarrow \quad k_{\upsilon\sigma\mathrm{f}} = \frac{\mathcal{R}_0}{\mathcal{R}'_{0\mathrm{f}}} = \frac{\mathcal{R}_0}{\Theta/\Phi_{0\mathrm{f}}} = \frac{\mathcal{R}^\sigma_\mathrm{gi}}{\mathcal{R}^\sigma_\mathrm{gi} + \mathcal{R}_{0\mathrm{gf}}} \frac{\mathcal{R}_0}{\mathcal{R}'_{0\mathrm{t}}}. \quad (13)$$

5.1 Comparison

Up to a frequency of 1 Hz the implementation of the force–related reluctance $\underline{\mathcal{R}}'_{\mathrm{eff\,f}}$ by means of the flux divider (10) or the correction factor $k_{\upsilon\sigma\mathrm{f}}$ (13) leads to equal results, as Fig. 8 illustrates. The absolute error in respect to the FEA can be reduced by 0.35 dB to < 0.1 dB (stationary) compared to the fringing/leakage–free $\underline{\mathcal{R}}_\mathrm{eff}$, at which point the simulatively determined reluctance is more accurate.

However, as opposed to the corrected total effective reluctance $\underline{\mathcal{R}}'_{\mathrm{eff\,t}}$ (cf. Fig. 6), the force–related reluctance $\mathcal{R}'_{\mathrm{eff\,f}}$, which is based on the flux divider, does not provide satisfying results in the relevant bandwidth up to 1 kHz. The reason for this derives from the the shift in the leakage flux distribution from the shaft to the coil for high frequencies, which cannot be modeled by the reluctance network. Although occurring errors cancel each other out for $\underline{\mathcal{R}}'_{\mathrm{eff\,t}}$, this is not the case for $\underline{\mathcal{R}}'_{\mathrm{eff\,f}}$ resulting in an inaccurate representation of the force–generating flux $\underline{\Phi}_\mathrm{f}$. On the other hand, compared to the original analytical solution the correction factor $k_{\upsilon\sigma\mathrm{f}}$ allows only a slight improvement in accuracy for $1\,\mathrm{Hz} < f < 1\,\mathrm{kHz}$ (Fig. 8), but more importantly does not degrade it. Hence we conclude, if the force–generating flux $\underline{\Phi}_\mathrm{f}$ is to be the focus, the correction factor is the preferred method.

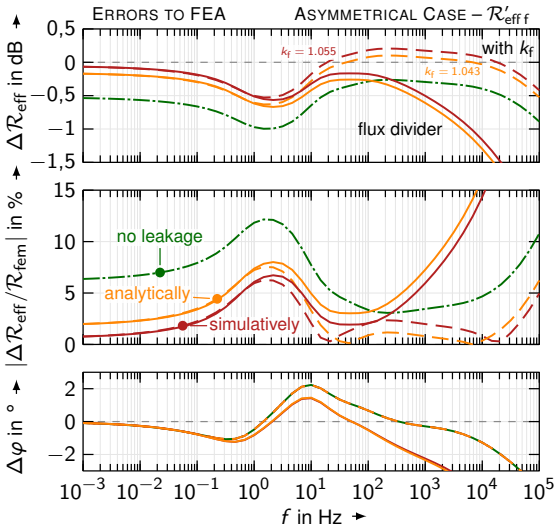

Figure 8: Absolute and relative magnitude and phase error for the force–generating reluctance $\mathcal{R}'_{\mathrm{eff\,f}}$ based on the flux divider (simplified reluctance network) or correction factor $k_{\upsilon\sigma\mathrm{f}}$ in respect to reference FEA

Furthermore, Fig. 8 reveals a possibly unexpected relation. The errors of $\left|\underline{\mathcal{R}}'_{\mathrm{eff\,f}}\right|$ in respect to $|\underline{\mathcal{R}}_\mathrm{eff}|$ are smaller than in the case of $\underline{\mathcal{R}}'_{\mathrm{eff\,t}}$ and remain negative. This in turn means that $\left|\underline{\mathcal{R}}'_{\mathrm{eff\,f}}\right|$ is smaller than $|\underline{\mathcal{R}}_\mathrm{eff}|$ and the force f is actually increased by the presence of fringing and leakage fluxes. Although, the force–generating flux $\underline{\Phi}_\mathrm{f}$ is indeed smaller than the total flux $\underline{\Phi}_\mathrm{t}$ (reduced by $\underline{\Phi}^\sigma$), the fringing and leakage fluxes cause a general reduction of the total reluctance $\left|\underline{\mathcal{R}}'_{\mathrm{eff\,t}}\right| \ll |\underline{\mathcal{R}}_\mathrm{eff}|$ and thus an increase of the actuator force. In our case the latter effect is dominant, resulting in correction factors $k_{\upsilon\sigma\mathrm{t|f}} > 1$. But it is important to note, that this observation cannot be generalized for all actuators or magnetic bearings and is only probable in case the force–generating fringing fluxes dominate over the leakage fluxes.

5.2 Correction of Flux Estimator

By recalling the definition of the flux estimator from (1), we see that there are multiple occurrences of the effective inductance $\underline{L}_\mathrm{eff}$ and its stationary counterpart $L_\mathrm{h} = \lim_{\omega\to 0} \underline{L}_\mathrm{eff}(\mathrm{j}\omega)$, the main inductance. While the first term is the actual force–related field building component, which we correct with the factor $k_{\upsilon\sigma\mathrm{f}}$, the second term describes the magnetizing currents, that relate to the total flux $\underline{\Phi}_\mathrm{t}$. Hence, the latter has to be corrected with the factor $k_{\upsilon\sigma\mathrm{t}}$ finally leading to:

$$\underline{G}'_\mathrm{FE}(\mathrm{j}\omega) = \frac{\underline{\Phi}_{\mathrm{f\,est}}(\mathrm{j}\omega)}{\underline{i}_\mathrm{meas}(\mathrm{j}\omega)} = \underbrace{\frac{L_\mathrm{hf}}{N}}_{\substack{\textit{force–related:}\\ \text{field}}} \cdot \overbrace{\frac{R_\mathrm{Cu} + s\underline{L}_{\mathrm{eff\,t}}(\mathrm{j}\omega)}{\underbrace{R_\mathrm{Cu} + sL_\mathrm{ht}}_{\text{magnetizing current}}}}^{\substack{\textit{measurable:}\\ \text{magnetizing current}}}, \quad (14)$$

Whether or not this differentiation is appropriate depends on the actuator geometry and the balance between fringing and leakage fluxes. In our case $k_{\upsilon\sigma\mathrm{f}}$ and $k_{\upsilon\sigma\mathrm{t}}$ differ by considerable 5.2 % and its inclusion comes at no cost. We note, that in fact the main inductances L_ht and L_hf are not directly affected by the magnetic skin effect, but by the redistribution of the fringing/leakage fluxes. We still assume them to be constant. Theoretically, it would be possible to isolate the frequency–dependent influence of these non–core fluxes and project them on the main inductances as well. However, the improvement would be very low compared to the additional computing effort.

6. Conclusion and outlook

The control of electromagnetic actuators and magnetic bearings usually relies on simplified models and perturbations like eddy currents, hysteresis, saturation, fringing and leakage fluxes are omitted. Especially in case of nonlaminated cores, it is widely accepted that eddy currents have a significant impact on the actuators performance and should be considered within the design of the control. In previous works we laid the groundwork for the first practical digital implementation of a flux estimator to fully compensate eddy currents in the inner actuator control loop. The considerably minor perturbations fringing and leakage remain solely subjects of academic research. Although various studies exist, they are usually limited to the analytical modeling and FE–analyses of the actuator. For the first time, we discussed the actual applicability of the known analytical models to control design and further improved them.

Our study regarding the fringing and leakage fluxes in a magnetic thrust bearing shows, that the practicality of a reluctance network highly depends on whether the total flux $\underline{\Phi}_\mathrm{t}$ and its respective corrected total reluctance $\underline{\mathcal{R}}'_{\mathrm{eff\,t}}$ is of interest or the actual force–generating flux $\underline{\Phi}_\mathrm{f}$ relating to $\underline{\mathcal{R}}'_{\mathrm{eff\,f}}$. In the former case, the proposed networks can significantly reduce model errors (static: 11.8 %) by 10 percentage points over a wide range of frequencies. The full reluctance network is only beneficial over the simplified network for less relevant frequencies above 1 kHz, where the characteristic phase drop is reproduced. In the bandwidth of interest below 1 kHz both networks are equally accurate. In the latter case, due to the magnetic skin effect, neither the full nor the simplified reluctance network can model the changing flux distribution for frequencies above 1 Hz, leading to an incorrect representation of the force-generating flux $\underline{\Phi}_\mathrm{f}$ and its according reluctance $\underline{\mathcal{R}}_{\mathrm{eff\,f}}$. However, constant correction factors, possibly greater than 1, reduce the model errors (static: 6.4 %) by satisfying 5.6 percentage points. Since they do not increase the system order and are most simple to implement we deem them to be the preferred variant for the flux estimator and control models in general.

We conclude, that our findings in this article only slightly improve the previously proposed flux control based on a fractional–order flux estimator. However, for the commonly omitted and supposedly minor perturbations fringing and leakage fluxes, we provided an extensive review about modeling approaches and discussed their impact as well as practical applicability as reference for future studies.

References

Feeley, J. J. (1996). “A simple dynamic model for eddy currents in a magnetic actuator”. *IEEE Transactions on Magnetics* 32.2, pp. 453–458.

Ferreira, J., E. Maslen, and R. Fittro (2017). “Transpermeance Amplifier Applied to Magnetic Bearings”. *Actuators* 6.9, pp. 1–20.

Keith, F. J. (1993). “Implicit flux feedback control for magnetic bearings”. English. Dissertation. University of Virginia.

Kucera, L. and M. Ahrens (1996). “A Model for Axial Magnetic Bearings Including Eddy Currents”. *3rd International Symposium on Magnetic Suspension Technology*. .2. Tallahassee, United States: NASA, pp. 421–437.

Le, Y. and K. Wang (2016). “Design and Optimization Method of Magnetic Bearing for High-Speed Motor Considering Eddy Current Effects”. *IEEE/ASME Transactions on Mechatronics* 21.4, pp. 2061–2072.

Meeker, D. C., E. H. Maslen, and M. D. Noh (1996). “An augmented circuit model for magnetic bearings including eddy currents, fringing, and leakage”. *IEEE Transactions on Magnetics* 32.4, pp. 3219–3227.

Rabinovici, R. and B. Kaplan (1992). “Effective magnetization and forces due to eddy currents”. *IEEE Transactions on Magnetics* 28.3, pp. 1863–1869.

Seifert, R. and W. Hofmann (2021a). “Highly Dynamic Thrust Bearing Control Based on a Fractional-Order Flux Estimator”. *IEEE Transactions on Industry Applications* 57.6, pp. 6988–6999.

Seifert, R., J. Porstmann, and W. Hofmann (2021b). “Consideration of Hysteresis, Saturation, Fringing and Leakage Fluxes in the Frequency–Dependent Analytical Model of Nonlaminated Cylindrical Actuators”. *IEEE TechRxiv*. Preprint, pp. 1–17.

Seifert, R., K. Röbenack, and W. Hofmann (2019). “Rational Approximation of the Analytical Model of Nonlaminated Cylindrical Magnetic Actuators for Flux Estimation and Control”. *IEEE Transactions on Magnetics* 55.12, pp. 1–16.

Stoll, R. (1974). *The analysis of eddy currents*. Monographs in electrical and electronic engineering. Oxford: Clarendon Press.

Sun, Y., Y.-S. Ho, and L. Yu (2009). “Dynamic Stiffnesses of Active Magnetic Thrust Bearing Including Eddy-Current Effects”. *IEEE Transactions on Magnetics* 45.1, pp. 139–149.

Vischer, D. (1988). “Sensorlose und spannungsgesteuerte Magnetlager”. Dissertation. ETH Zürich.

Wang, K., D. Wang, H. Lin, Y. Shen, X. Zhang, and H. Yang (2014). “Analytical Modeling of Permanent Magnet Biased Axial Magnetic Bearing With Multiple Air Gaps”. *IEEE Transactions on Magnetics* 50.11, pp. 1–4.

Zhong, Y., L. Wu, X. Huang, Y. Fang, and J. Zhang (2017). “An Improved Magnetic Circuit Model of a 3-DOF Magnetic Bearing Considering Leakage and Cross-Coupling Effects”. *IEEE Transactions on Magnetics* 53.11, pp. 1–6.

Zhu, L. and C. Knospe (2010). “Modeling of Nonlaminated Electromagnetic Suspension Systems”. *IEEE Transactions on Mechatronics* 15.1, pp. 59–69.